Available online at www.sciencedirect.com
ScienceDirect
Trans. Nonferrous Met. Soc. China 28(2018) 1123−1131
Transactions of Nonferrous Metals Society of China
www.tnmsc.cn

Microstructure and textural evolution during cold rolling and annealing of commercially pure titanium sheet

Na LIU[1], Ying WANG[1,2], Wei-jun HE[1], Jun LI[2], Adrien CHAPUIS[1], Bai-feng LUAN[1], Qing LIU[1]

1. College of Materials Science and Engineering, Chongqing University, Chongqing 400044, China;
2. Pangang Group Research Institute Co., Ltd., Chengdu 610031, China

Received 12 January 2017; accepted 18 July 2017

Abstract: The effects of cold rolling and annealing on the microstructure and textural evolution of a commercially pure titanium (CP-Ti) sheet were investigated. Electron backscatter diffractometry demonstrates that the deformation during rolling is accommodated by twinning and slip. Additionally, twinning is the dominant deformation mechanism when the cold rolling reduction is less than 40%. During rolling, $\{11\bar{2}2\}\langle 11\bar{2}3\rangle$ contraction twinning (CT) and $\{10\bar{1}2\}\langle 10\bar{1}1\rangle$ extension twinning (ET) are activated. And, the intensity of the (0002) pole along the ND gradually increases with increasing deformation. During annealing, the fraction of low angle grain boundaries (LAGBs) and the intensity of the (0002) pole along the ND gradually decrease slightly with increasing annealing time, while twinning lamellae disappear rapidly. When the annealing time reaches 60 min, 20% cold-rolled sheet recrystallizes almost completely.

Key words: commercially pure titanium; texture; twinning; cold rolling; recrystallization

1 Introduction

Titanium and its alloys with high specific strength, excellent corrosion resistance, durability at elevated temperature, acceptable castability, good weldability, and excellent biocompatibility play a significant role in various industries [1]. Studies on deformation and recrystallization in hexagonal close-packed metals have gained importance in the recent years [2,3]. Hexagonal close-packed metals, such as titanium, primarily deform by slip and twinning [4,5]. The specific deformation mechanisms in metals with a hexagonal close-packed crystal structure are less well understood than those in cubic metals because of their large number of independent slip systems. In commercially pure Ti (CP-Ti), slip occurs mainly with dislocations of the $\langle a\rangle$ Burgers vector in prismatic planes [6]. Since the Von Mises criteria for plastic deformation require five independent slip systems, deformation by a $\langle c+a\rangle$ slip on pyramidal planes or by twinning needs to be activated [7,8]. Twinning is reported to be more easily activated under compressive stress than tensile stress [9].

Deformation twinning is an important deformation mode for pure titanium. CHRISTIAN and MAHAJAN [10] analyzed the twinning of hexagonal close-packed crystals. QIN et al [11,12], WANG et al [13], HAMA et al [14] and LI et al [15] studied the twinning behavior and twinning systems of pure titanium during plastic deformation. GHADERI and BARNETT [16] observed that the volume fraction and length of twinning lamellae are strongly dependent on the grain size of pure titanium. This reduction in grain size inhibits further twinning at large deformations and results in a stable textural evolution controlled exclusively by dislocation slips. CONTIERI et al [17] analyzed the activation energy for recrystallization and grain growth kinetics of CP-Ti. WAGNER et al [18], HAYAMA and SANDIM [19] studied the annealing behavior and the recrystallization texture in large reduction of cold rolling titanium sheets.

However, for the low to medium levels of deformation, the annealing behavior and the recrystallization have seldom been reported. Moreover, the evolution of lamellar twinning during annealing has seldom been reported. In addition, recent advances in electron back-scattered diffraction (EBSD) techniques provide a powerful method to analyze the deformation twinning and texture in CP-Ti. Thus, the objective of the

Foundation item: Projects (51505046, 51421001) supported by the National Natural Science Foundation of China
Corresponding author: Wei-jun HE; Tel: +86-23-65106067; E-mail: weijun.he@cqu.edu.cn
DOI: 10.1016/S1003-6326(18)64748-X

present work was to study the deformation twinning and textural evolution of CP-Ti during cold rolling and annealing.

2 Experimental

The as-received CP-Ti sheet, 230 mm (length) × 60 mm (width) × 4.6 mm (height), was produced by hot rolling and annealing. The chemical composition of the as-received CP-Ti sheets is given in Table 1. To investigate the microstructural and textural evolution during plastic deformation, the as-received CP-Ti sheets were cold rolled by 10%, 20%, 30% and 40%. To characterize the microstructural evolution of the CP-Ti sheet during annealing, the 20% reduced specimen was annealed at 550 °C in a muffle furnace for 5, 10, 20, 30 and 60 min.

All the specimens were examined using a TESCAN MIRA3 field emission scanning electron microscope with a normal EBSD detector operating at 20 kV. For EBSD analysis, specimens were prepared by electrolytic polishing in a solution of 10 mL perchloric acid and 90 mL methanol at 17 V and −30 °C. All EBSD data were collected at a 0.3 μm step size scan of a 150 μm×150 μm area on a surface containing the rolling direction (RD) and the normal direction (ND), and the data were processed with the HKL Channel 5 software from HKL Technology.

Table 1 Chemical composition of commercially pure titanium (mass fraction, %)

Fe	O	N	C	Ti
0.02	0.039	0.003	0.013	Bal.

3 Results and discussion

3.1 Starting material

In Fig. 1, the EBSD data show that the as-received sheet is recrystallized. The average grain size is ~10 μm (Fig. 1(a)). No twinning is found in the as-received sample, as indicated in Fig. 1(b). As shown in Fig. 1(c), the (0002) pole figure of the initial texture reveals a bimodal distribution along the *c*-axis. More specifically, most grains are oriented along the normal direction (ND) with a spread of ±50° toward the transverse direction (TD). There is no preferential distribution of the prismatic planes.

The misorientation angle distribution is displayed in Fig. 1(d). To facilitate discussion in the following text, grain boundaries with misorientations lower and higher

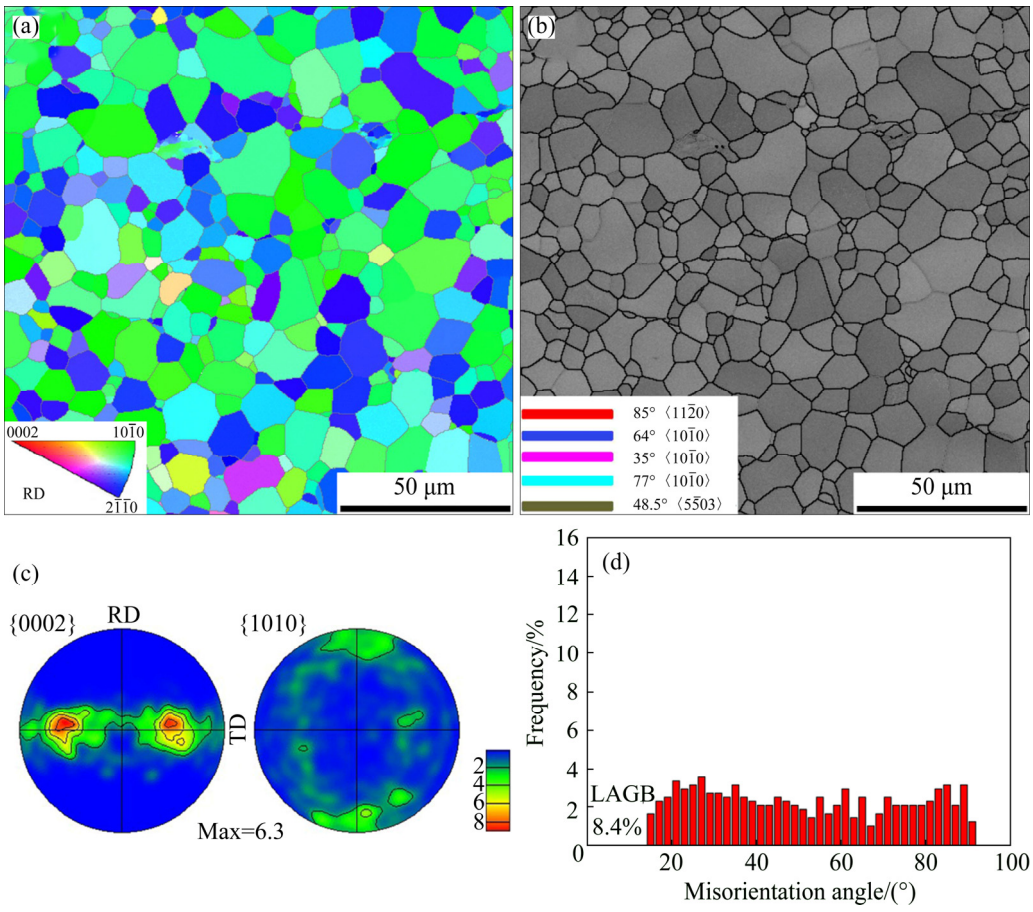

Fig. 1 EBSD inverse pole figure (IPF) map (a), image quality (IQ) map (b), pole figure (c) and misorientation angle distribution (d) of as-received commercial purity titanium sheets

than 15° are denoted as low angle grain boundaries (LAGBs) and high angle grain boundaries (HAGBs), respectively. In the as-received sample, the HAGBs account for a large proportion (91.6%) of the boundaries compared with the LAGBs (8.4%), as displayed in Fig. 1(d). Therefore, the structure of the as-received sample is uniform and almost entirely composed of HAGBs.

3.2 Microstructure evolution during cold rolling

EBSD was expected to reveal further microstructural characteristics. For example, EBSD is able to identify twinning types and quantitatively determine the proportion of each type. The microstructural evolution of the CP-Ti sheet during cold rolling is shown in Fig. 2. In all four rolled samples, $\{11\bar{2}2\}\langle 11\bar{2}\bar{3}\rangle$ contraction twinning and $\{10\bar{1}2\}\langle 10\bar{1}1\rangle$ extension twinning were activated, as indicated by the blue lines and red lines, respectively, in the image quality (IQ) maps. When the reduction is 10%, contraction twins are the main type of twinning, as shown in Fig. 2(a). Only a few extension twins are observed at this

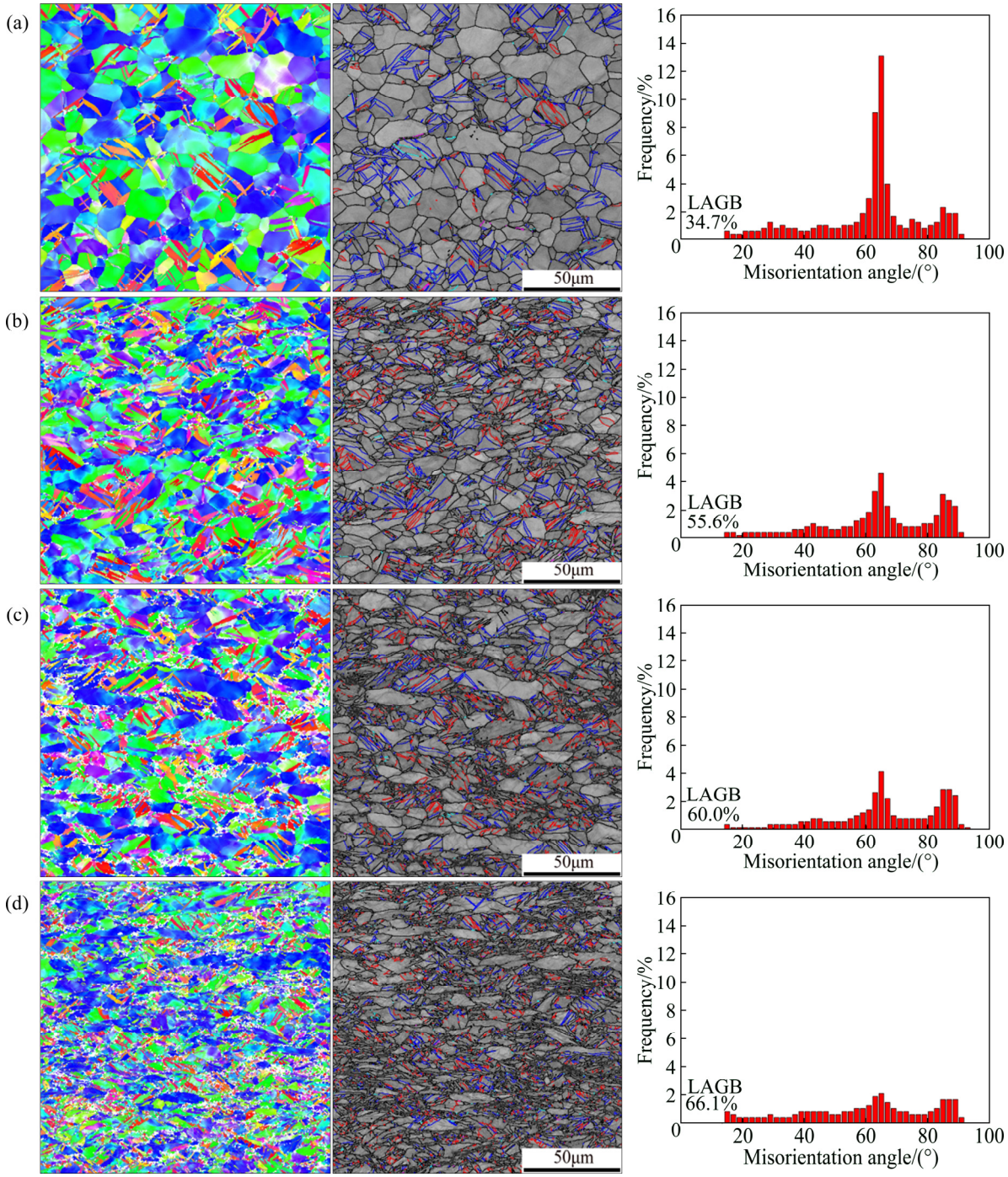

Fig. 2 EBSD IPF maps, IQ maps and misorientation angle distributions of cold-rolled samples with different reductions: (a) 10%; (b) 20%; (c) 30%; (d) 40%

deformation level. When the deformation is increased to 20%, many extension twins are activated, as shown in Fig. 2(b). The combination of the initial texture and the deformation state imposed during cold rolling results in the preferential activation of contraction twinning. Most grains are twinned above 20% deformation and a few untwinned grains were significantly longer than the twinned grains. For reductions of 30% and 40%, most of the grains are obviously elongated along the RD and a significant grain refinement is observed.

This grain refinement is mainly induced by twinning. With increasing deformation, the grains are gradually broken and refined due to twinning generation. In these grains, the crossing of deformation twins and the generation of secondary and tertiary twins cause the development of a twinned lamellar structure. The thickness of these twinned lamellae is several micrometers, which is a significantly finer structure compared with the initial grain size.

The misorientation angle distributions of the cold rolled CP-Ti were determined from the EBSD data, as shown in Fig. 2. The misorientation angle distributions show local maxima in the range of 60°−65°, which is attributed to a significant proportion of $\{11\bar{2}2\}$ contraction twin boundaries (corresponding to 65° $\langle 10\bar{1}0\rangle$ boundaries). The misorientation angle distribution also displays a local maximum approximately 85°, which is attributed to $\{10\bar{1}2\}$ extension twins (corresponding to 85° $\langle 11\bar{2}0\rangle$ boundaries). For rolling reductions less than 20%, the boundaries near 65° were predominant. Compared with the as-received materials (see Fig. 1), LAGBs account for a large proportion of the grain boundaries. Specifically, LAGBs account for 34.7% of all grain boundaries in the 10% reduction sample and increase significantly to 66.1% after a 40% reduction. This finding implies that the profuse accumulation of dislocations is due to high slip activation during rolling deformation. However, when larger reductions further decrease the number of high-angle boundaries, the fractions of boundaries near 65° and 85° remain high relative to the fraction of other high angle boundaries. At a 10% reduction, the misorientation angle distribution exhibits sharp peaks approximately 65° and 85°, but they are broadened with larger rolling reductions.

3.3 Microstructural evolution during annealing

Figure 3 displays the microstructure of the 20% cold-rolled sample after different annealing time. After the sample is annealed for 5 min, the morphology, grain shapes and quantity of twins are basically unchanged. After 10 min, some small recrystallized grains are found and the quantity of twins begins to decrease. As the annealing time is increased to 20 and 30 min, the quantity of twins significantly decreases and the recrystallized grains grow larger. An equiaxed grain structure replaces the deformed structure at 60 min of annealing (Fig. 3(e)), which means that the recrystallization is basically complete. The average grain size of the recrystallized microstructure is ~10 μm, which is close to the initial grain size.

The misorientation angle distributions of the annealed samples are also displayed in Fig. 3. It can be seen that the sharp peaks at approximately 65° and 85° gradually decrease and finally disappear with increase in the annealing time. This is related to the reduction of $\{11\bar{2}2\}$ contraction twins and $\{10\bar{1}2\}$ extension twins during annealing. After annealing for 5 and 10 min, LAGBs do not diminish, and they still account for a large fraction of grain boundaries compared with the cold-rolled sample. However, it is expected that some recovery and rearrangement of dislocations occur. As the annealing time increases to 20 and 30 min, the percent of LAGBs decreases slightly while the quantity of twins is reduced significantly. This suggests that the twins are consumed by recrystallized grains faster than by the deformed matrix during annealing. When the annealing time reaches 60 min, the fraction of LAGBs is reduced significantly. As shown in Fig. 4, the deformed grains have disappeared and the recrystallized grains account for 90% of all grains.

3.4 Textural evolution

The as-received sheets have a typical bimodal basal texture, in which the *c*-axis is tilted toward the transverse direction (TD). The $\{0002\}$ and $\langle 10\bar{1}0\rangle$ pole figures of the titanium sheet at different rolling reductions are shown in Fig. 5. The intensity of the (0002) pole along the TD is strengthened first and then weakened with increasing rolling deformations. However, the intensity of the (0002) pole along the ND gradually increases with increasing deformation. The intensity changes in the (0002) pole along the TD and ND are attributed to the activation of contraction twins and extension twins, respectively. Unlike the distribution of the basal planes, the maximum intensity for the prismatic planes, although not very strong, is found along the RD and is slightly affected by cold rolling deformation.

The $\{0002\}$ and $\{10\bar{1}2\}$ pole figures of the CP-Ti sheet during annealing are displayed in Fig. 6. As annealing time increases, the intensity of the $\{0002\}$ pole along the ND decreases gradually. After annealing for 60 min, the pole distribution becomes split-bimodal basal. However, some *c*-axes are still orientated toward the TD, even after annealing for 60 min. Qualitatively, these grains with a *c*-axis close to the TD are more common after annealing than in either the as-received sheet or the 20%-reduced sheet. This suggests that some

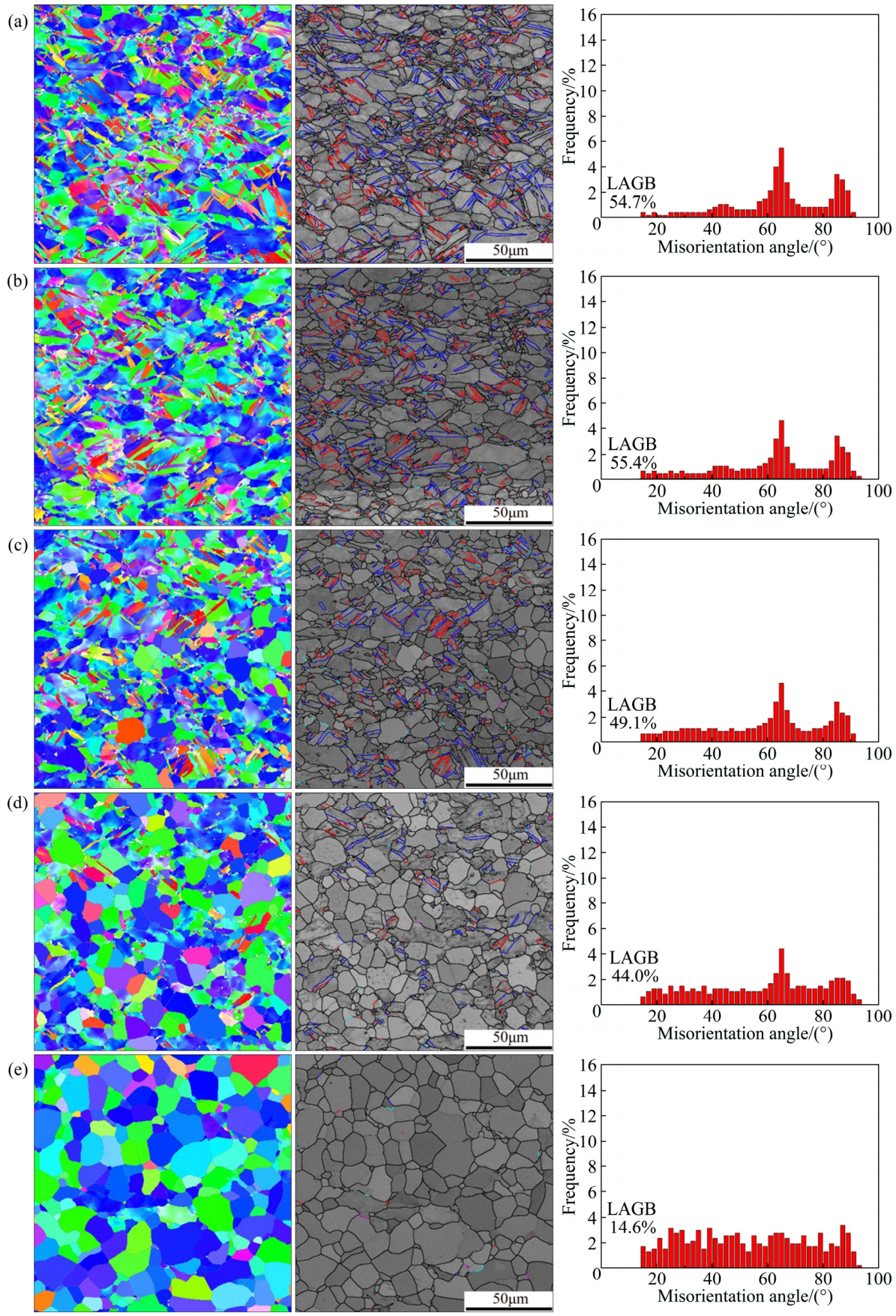

Fig. 3 EBSD IPF maps, IQ maps and misorientation angle distributions after annealing of 20% reduction sample at 550 °C for various time: (a) 5 min; (b) 10 min; (c) 20 min; (d) 30 min; (e) 60 min

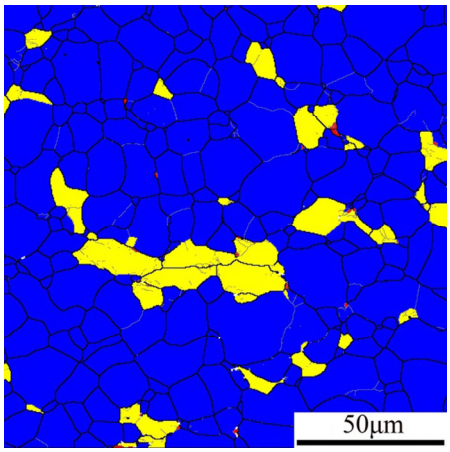

Fig. 4 EBSD IPF map after annealing at 550 °C for 60 min (Recrystallized grains are in blue, grains with sub-structure are in yellow and deformed grains are in red)

contraction twins become recrystallized grains while the extension twins disappear during annealing [20]. In keeping with observations made during cold rolling, the $\{10\bar{1}2\}$ twins do not obviously affect the texture during annealing.

3.5 Statistics and analyses of twin area fraction

To investigate twinning, a quantitative analysis of the twin area fraction was performed. Twin area fraction statistics at different rolling deformations and annealing times are given in Table 2 and Table 3, respectively. When the rolling deformation is 10%, the $\{11\bar{2}2\}\langle 11\bar{2}3\rangle$ compression twins are the main type of twins and represent 12.77% of the observed area, while, extension twins account for just 1.54%. At 20% rolling deformation, the area fraction of the $\{10\bar{1}2\}\langle 10\bar{1}1\rangle$

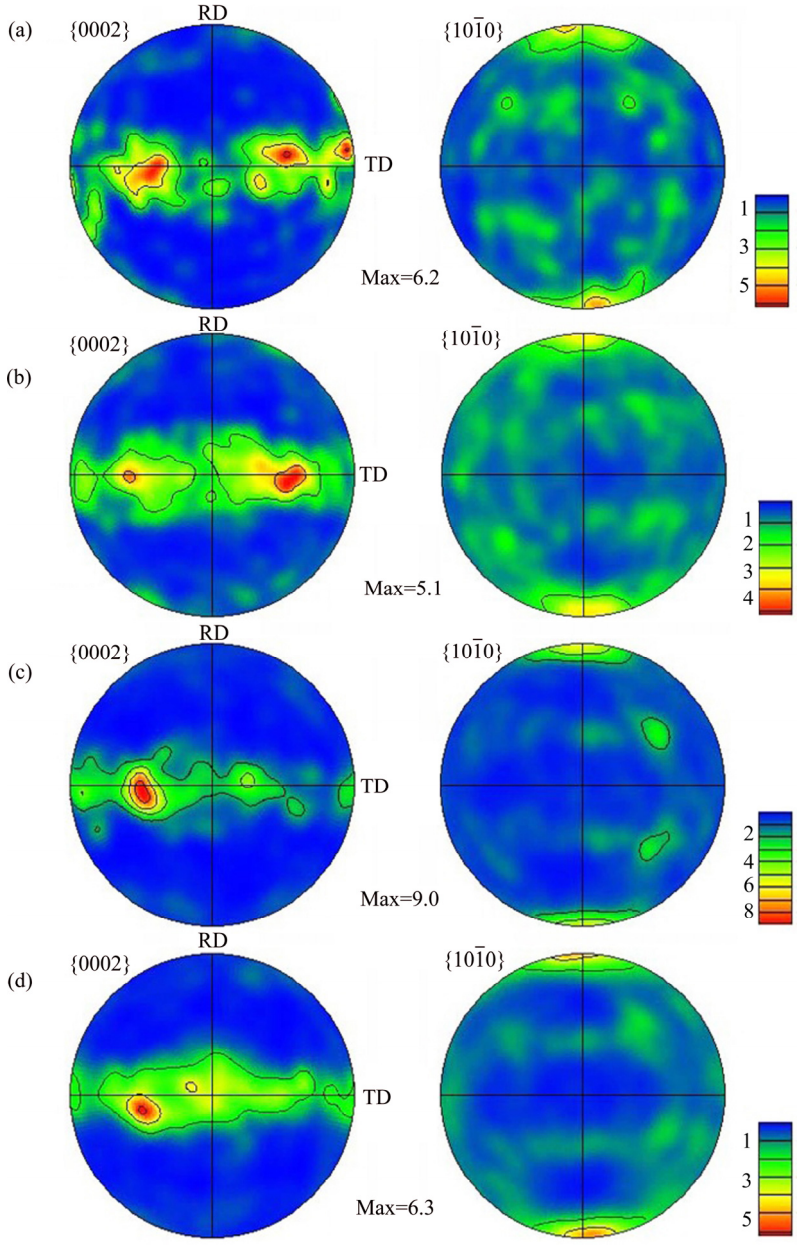

Fig. 5 Pole figures of cold-rolled CP-Ti at different reductions: (a) 10%; (b) 20%; (c) 30%; (d) 40%

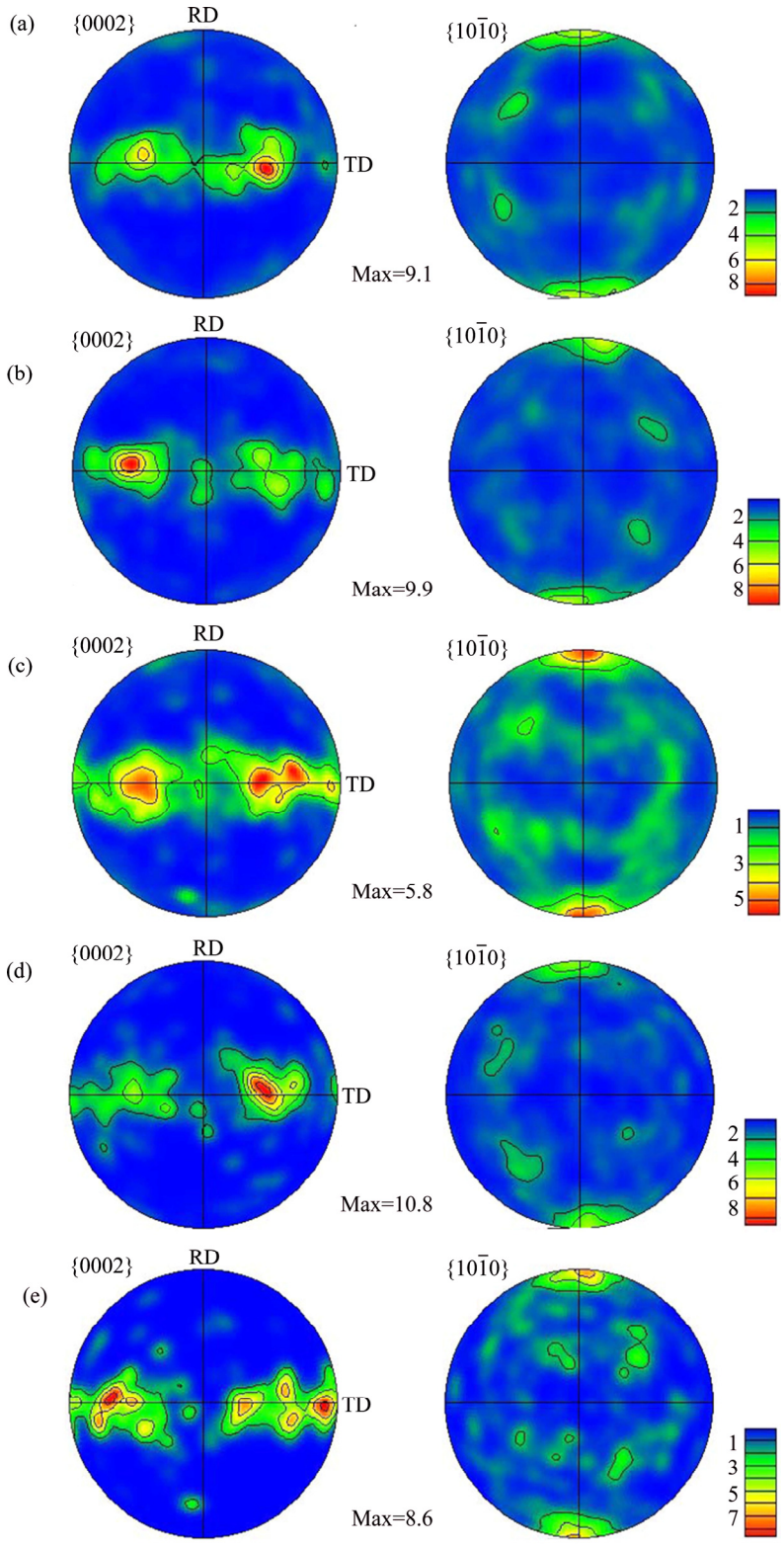

Fig. 6 Pole figures of 20% cold-rolled titanium after annealing at 550 °C for different time: (a) 5 min; (b) 10 min; (c) 20 min; (d) 30 min; (e) 60 min

extension twins increases substantially and reaches 6.77%. Meanwhile, the $\{11\bar{2}2\}\langle 11\bar{2}3\rangle$ compression twins remain at almost the same proportion as that after 10% rolling. The compression twins may reach saturation at 20% deformation. The nucleation of new compression twins may be prevented by extension twins. When the rolling deformation reaches 30% and 40%, the statistical proportion of both the compression and extension twins is significantly reduced. However, the twin area fraction does not necessarily decrease as the

reduction increases 30% or 40%. The number of non-indexed pixels near the twin boundaries increases with additional cold rolling (Fig. 2), which results in a decrease in the statistical twin area fraction. Additionally, this might arise from a destruction of the relationship between twins and matrix orientation, caused by dislocation slipping at the twin boundary, so that twins remain but are not identified as twins anymore. Once the misorientation diverges from the ideal value, the twin boundary cannot be identified.

Table 2 Twin area fraction at different cold rolling reductions

Type	Angle and axis	Twin area fraction/%			
		10%	20%	30%	40%
CT	65°⟨11$\bar{2}$2⟩	12.77	12.60	7.62	5.05
ET	85°⟨10$\bar{1}$2⟩	1.54	6.77	5.74	4.26
Total	−	14.31	19.37	13.36	9.31

Table 3 Twin area fraction of 20% reduction sample annealed for different durations

Type	Axial and angle	Twin area of fraction/%				
		5 min	10 min	20 min	30 min	60 min
CT	65°⟨11$\bar{2}$2⟩	12.48	8.22	6.24	3.36	<0.01
ET	85°⟨10$\bar{1}$2⟩	7.42	4.99	4.20	1.20	<0.01
Total	−	19.90	13.21	10.44	4.56	<0.01

As shown in Table 3, the twin area fractions of CT and ET decrease with increasing annealing time. After annealing for 5 min, the twin area fraction remains almost the same as that before annealing. As the annealing time increases from 10 to 30 min, the area fractions of compression twinning and extension twinning rapidly decrease. After annealing for 60 min, no twin lamella can be found.

3.6 Hardness evolution

The hardness of titanium sheets at different rolling deformations and annealing time is measured and shown in Fig. 7. While rolling deformation increases from 0% to 40%, the Vickers hardness value increases from HV 122 to HV 185. The hardening of the material may be caused by the high density of dislocations, the increasing of twin boundary and grain refinement. As the deformation increases, the increased fraction of LAGBs indicates the increased dislocation density, which results in the work hardening of cold-rolled sheets. Additionally, the existing twins cause the grains refinement and inhibit the dislocation motion, which leads to the increased hardness. Figure 7(b) indicates that the hardness decreases from HV 185 to HV 115 as the annealing time increases from 0 to 60 min. The softening of the sheet corresponds to recrystallization and grain coarsening. The 5 min before the observed decrease confirms that annealing is an activated process. As the annealing time increases to 20 and 30 min, the quantity of twins and the percent of LAGBs decrease, which results in the significant decrease of hardness.

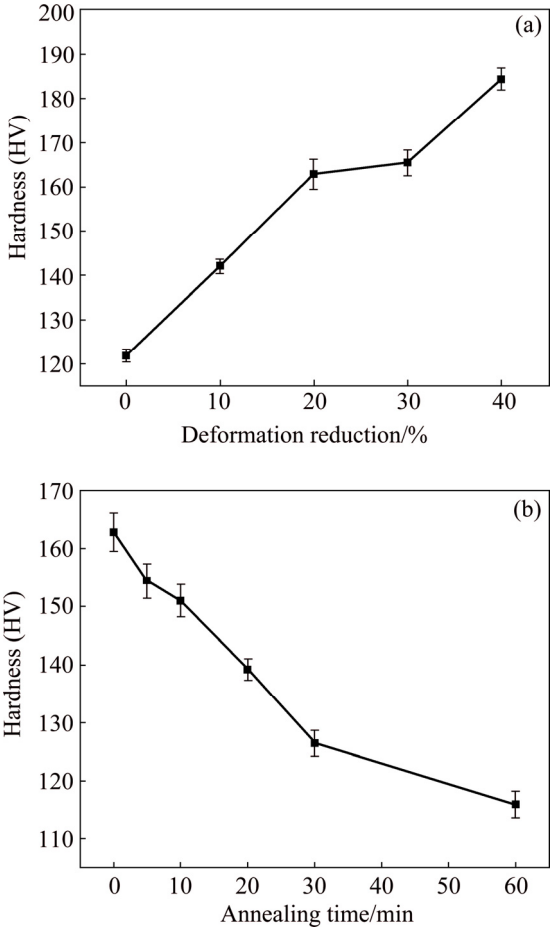

Fig. 7 Hardness evolution of samples: (a) Cold rolled; (b) Annealed

4 Conclusions

1) During the cold rolling of CP-Ti sheets, deformation is accommodated by slip and twinning. Initially, twinning is the dominant deformation mechanism of cold rolling deformation. At large rolling deformations (e.g., 40%), slip becomes the main deformation mechanism.

2) The cold rolling of CP-Ti sheets activates $\{11\bar{2}2\}\langle 11\bar{2}3\rangle$ compression twinning, often as primary twinning, but $\{10\bar{1}2\}\langle 10\bar{1}1\rangle$ extension twinning is also observed.

3) The intensity of the (0002) pole along the ND gradually increases with increasing deformation degree. However, with increasing annealing time, the intensity gradually decreases.

4) Recrystallization is almost complete when the annealing time reaches 60 min. The fraction of the

LAGBs begins to decrease significantly after twins disappear.

References

[1] ROODPOSHTI P S, SARKAR N F A, MURTY K L. Microstructural approach to equal channel angular processing of commercially pure titanium—A review [J]. Transactions of Nonferrous Metals Society of China, 2015, 25(5): 1353−1366.

[2] XU Xing, DONG Li-ming, BA Hong-bo, ZHANG Zhi-qiang, YANG Rui. Hot deformation behavior and microstructural evolution of beta C titanium alloy in β phase field [J]. Transactions of Nonferrous Metals Society of China, 2016, 26(5): 2874−2882.

[3] LI Cui, LI Bin, WU Ze-feng, QI Xiao-yong, YE Bing, WANG Ai-hua. Stitch welding of Ti−6Al−4V titanium alloy by fiber laser [J]. Transactions of Nonferrous Metals Society of China, 2017, 27(1): 97−101.

[4] ZHANG Xu-hu, TANG Bin, ZHANG Xia-lu, KOU Hong-chao, LI Jin-shan, ZHOU Lian. Microstructure and texture of commercially pure titanium in cold deep drawing [J]. Transactions of Nonferrous Metals Society of China, 2012, 22(3): 496−502.

[5] YANG Yong-biao, WANG Fu-chi, TAN Cheng-wen, WU Yuan-yuan, CAI Hong-nian. Plastic deformation mechanisms of AZ31 magnesium alloy under high strain rate compression [J]. Transactions of Nonferrous Metals Society of China, 2008, 18(5): 1043−1046.

[6] CHUN Y B, YU S H, SEMIATIN S L, HWANG S K. Effect of deformation twinning on microstructure and texture evolution during cold rolling of CP-titanium [J]. Materials Science and Engineering A, 2005, 398(1−2): 209−219.

[7] TEGART W J M. Independent slip systems and ductility of hexagonal polycrystals [J]. Philosophical Magazine, 1964, 9(98): 339−341.

[8] CHUN Y B, HWANG S K, KIM M H, KWUN S I, CHAE S W. Effect of Mo addition on the crystal texture and deformation twin formation in Zr-based alloys [J]. Journal of Nuclear Materials, 2001, 295(1): 31−41.

[9] LI Hong-wei, ZHANG Xia-lu, CHEN Jia-yuan, LI Jin-shan. Effects of stress state on texture and microstructure in cold drawing-bulging of CP-Ti sheet [J]. Transactions of Nonferrous Metals Society of China, 2013, 23(1): 23−31.

[10] CHRISTIAN J W, MAHAJAN S. Deformation twinning [J]. Progress of Materials Science, 1995, 39(1−2): 1−157.

[11] QIN Hong, JONAS J J. Variant selection during secondary and tertiary twinning in pure titanium [J]. Acta Materialia, 2014, 75: 198−211.

[12] QIN Hong, JONAS J J, YU Hong-bing, BRODUSCH N, GAUVIN R, ZHANG Xi-yan. Initiation and accommodation of primary twins in high-purity titanium [J]. Acta Materialia, 2014, 71: 293−305.

[13] WANG Tong-bo, LI Bo-long, LI Mian, LI Ying-chao, WANG Zhen-qiang, NIE Zuo-ren. Effects of strain rates on deformation twinning behavior in α-titanium [J]. Materials Characterization, 2015, 106: 218−225.

[14] HAMA T, NAGAO H, KOBUKI A, FUJIMOTO H, TAKUDA H. Work-hardening and twinning behavior in a commercially pure titanium sheet under various loading paths [J]. Materials Science and Engineering A, 2015, 620: 390−398.

[15] LI X, DUAN Y L, XU G F, PENG X Y, DAI C, ZHANG L G, LI Z. EBSD characterization of twinning in cold-rolled CP-Ti [J]. Materials Characterization, 2013, 84: 41−47.

[16] GHADERI A, BARNETT M R. Sensitivity of deformation twinning to grain size in titanium and magnesium [J]. Acta Materialia, 2011, 59(20): 7824−7839.

[17] CONTIERI R J, ZANOTELLO M, CARAM R. Recrystallization and grain growth in highly cold worked CP-Titanium [J]. Materials Science and Engineering A, 2010, 527(16−17): 3994−4000.

[18] WAGNER F, BOZZOLO N, van LANDUYT O, GROSDIDIER T. Evolution of recrystallisation texture and microstructure in low alloyed titanium sheets [J]. Acta Materialia, 2002, 50(5): 1245−1259.

[19] HAYAMA A O F, SANDIM H R Z. Annealing behavior of coarse-grained titanium deformed by cold rolling [J]. Materials Science and Engineering A, 2006, 418(1−2): 182−192.

[20] XIN Yun-chang, ZHOU Hua, WU Gui-lin, CHAPUIS A, LIU Qing. A twin size effect on thermally activated twin boundary migration in a Mg−3Al−1Zn alloy [J]. Materials Science and Engineering A, 2015, 639: 534−539.

工业纯钛板材在冷轧和退火过程中的显微组织与织构演变

刘 娜[1]，王 莹[1,2]，何维均[1]，李 军[2]，Adrien CHAPUIS[1]，栾佰峰[1]，刘 庆[1]

1. 重庆大学 材料科学与工程学院，重庆 400044；
2. 攀钢集团研究院有限公司，成都 610031

摘 要：研究了工业纯钛板材在冷轧和退火过程中的显微组织与织构演变。电子背散射衍射结果表明，在冷轧条件下的塑性变形由孪生和滑移共同协调作用。当压下量小于 40%时，其主要的塑性变形方式为形变孪生。在轧制过程中，同时产生了 $\{11\bar{2}2\}\langle 11\bar{2}3\rangle$ 压缩孪晶和 $\{10\bar{1}2\}\langle 10\bar{1}1\rangle$ 拉伸孪晶；而且，沿 TD 方向的织构强度随变形量增加逐渐增强。在退火过程中，随着退火时间的延长，小角度晶界缓慢减少而孪晶片层快速消失，沿 TD 方向的织构强度逐渐减弱。当退火时间延长至 60 min 时，压下量 20%的样品已经完全再结晶。

关键词：工业纯钛；织构；孪晶；冷轧；再结晶

(Edited by Bing YANG)